Electronic Research Archive

https://www.aimspress.com/journal/era

ERA, 34(2): 1079–1094.
DOI: 10.3934/era.2026050
Received: 09 December 2025
Revised: 24 January 2026
Accepted: 28 January 2026
Published: 30 January 2026

Research article

Delayed feedback and sensitivity analysis for oscillations in Parkinson's disease

Quanbao Ji[1,2] **and Hongjian Meng**[1,*]

[1] School of Mathematical Sciences, Guangxi Minzu University, Nanning 530006, China

[2] Guangxi Key Laboratory of Universities Optimization Control and Engineering Calculation, Nanning 530006, China

* **Correspondence:** Email: menghj2000912@163.com.

Abstract: Pathological oscillations within the basal ganglia (BG) are a hallmark of Parkinson's disease (PD), a prevalent neurodegenerative disorder. This study aims to evaluate the effects of delayed feedback on oscillatory activity in a PD model and to analyze the roles of synaptic weights and transmission delays within the feedback circuit. Results indicate that the model induced by delayed feedback increase leads to the transition in firing activity, progressing from regular gamma activity to pathological beta oscillation states, and may even transition into complex states. This transition is further modulated by synaptic weights, which could not only change the model from a steady state to an oscillating state, but also cause a high-saturation steady state when sufficiently large. Furthermore, sensitivity analysis based on polynomial chaos expansions enables the quantification of the contributions of transmission delays and synaptic weights to the oscillation frequency variance of the model. The analysis shows that with increasing delayed feedback, the transmission delay parameter that contributes the most to model oscillation shifts from transmission delay within the BG circuit to that of the cerebral cortex circuit. Synaptic weights between the external globus pallidus and the subthalamic nucleus have a significant impact on oscillatory activity when delayed feedback is large. Our findings provide new directions for further clinical treatment of PD.

Keywords: Parkinson's disease; delayed feedback; oscillations; polynomial chaos expansion; sensitivity

1. Introduction

Parkinson's disease (PD), a progressive neurodegenerative condition, is primarily characterized by the depletion of dopaminergic neurons within the midbrain's substantia nigra, and it has displayed a rising trend in its point prevalence over the past few decades [1, 2]. The loss of nigral dopaminergic

neurons along with the presence of Lewy bodies in the perikarya of degenerating brainstem neurons are the hallmark lesions of PD [3, 4]. The function of the BG could be impaired by these hallmark lesions, leading to a spectrum of impairments. These encompass classic motor deficits such as limb tremor, bradykinesia, and hypomimia, as well as diverse non-motor issues such as cognitive decline, sleep disturbances, and sensory deficits [5, 6].

Currently, pharmacological treatment is commonly used to treat PD, but patients may experience anisocoria, fluctuating symptoms, and disease progression with increasing medication doses and types [7,8]. In contrast, deep brain stimulation (DBS) employs chronic and high-frequency stimulation of brain areas, enabling a reduction in clinical symptoms of PD and thereby alleviating medication requirements [9,10]. DBS represents a highly effective therapy not only for its clinical efficacy but also for the adjustability of its stimulation parameters, such as timing and intensity [11]. This adjustability facilitates the development of model-based closed-loop control strategies, underscoring the importance of theoretical research on mechanisms like delayed feedback control for advancing DBS from a static therapy toward a dynamic, adaptive intervention.

In research on delayed feedback for DBS, Rosenblum et al. first proposed a method based on mean field-based time-delayed feedback, which effectively controlled collective synchrony in globally coupled systems and oscillator networks by adjusting external delayed loop parameters [12, 13]. Popovych et al. developed a nonlinear delayed feedback control that achieved desynchronization in various oscillator networks and neuronal populations [14]. Research from Ji et al. indicated that their dynamic delayed feedback control (DDFC) could decrease self-synchronization in coupled neuronal oscillators and suppress the pathological beta oscillations observed in a model of PD [15, 16]. Yang et al. found that their introduced intermittent nonlinear differential delayed feedback scheme could mitigate abnormal synchronous oscillations in a built BG-thalamus network model [17]. However, it remains unclear whether there is an intrinsic correlation between the delayed feedback parameters and key pathological parameters of PD models, thereby hindering the construction of targeted therapeutic strategies for pathological oscillations.

Therefore, the aim of this study is to establish a Cortex-BG model under dynamic delayed feedback control, which includes extracellular DBS and the simulation of the dynamic mechanism of PD. This model is used to explore the intrinsic correlation between delayed feedback and pathological oscillations in PD and to examine how delayed feedback and PD parameters jointly determine the dynamic states and oscillation types of the system. Moreover, through employing Sobol's sensitivity analysis using polynomial chaos expansion, we not only elucidate the complex interplay between delayed feedback and Parkinsonian pathological oscillations but also provide quantitative insights into the sensitivity of DDFC control parameters in regulating pathological oscillations in PD. In Section 2, the specific structure of the model is described. The results of the numerical simulation and Sobol's sensitivity analysis are illustrated in Sections 3 and 4, respectively. Lastly, conclusions and a discussion are given in Section 5.

2. Model and methods

2.1. A physiological model for Parkinsonian dynamics

The Cortex-BG model established by Zeng et al. is utilized to reveal the dynamic mechanisms of the transition from normal to pathological rhythms in PD [18]. In this study, this model provides

the foundation for developing and evaluating closed-loop control strategies to suppress pathological rhythms. As shown in Figure 1, the Cortex-BG model consists of the cerebral cortex circuit and the BG circuit. Excitatory (E) and inhibitory (I) neuronal populations constitute the cerebral cortex circuit, while the BG circuit involves a neural loop encompassing the subthalamic nucleus (STN) along with the external and internal segments of the globus pallidus (GPe and GPi). The E driven by a constant external excitatory input, Con, releases glutamate that travels via a specific feedback channel to stimulate the STN. Within the BG circuit, the STN acts as a central hub. The GPe and GPi receive excitatory signals (glutamatergic) from afferents in the STN. They also integrate a constant inhibitory input (GABAergic) from the striatum (Str). As for the GPi and STN, they are connected via inhibitory (GABAergic) afferent pathways to the GPe. Consequently, a core STN–GPe excitatory–inhibitory feedback loop is formed. The GPi integrates three primary inputs: an excitatory connection from the STN, an inhibitory connection from the GPe, and an inhibitory connection from the Str.

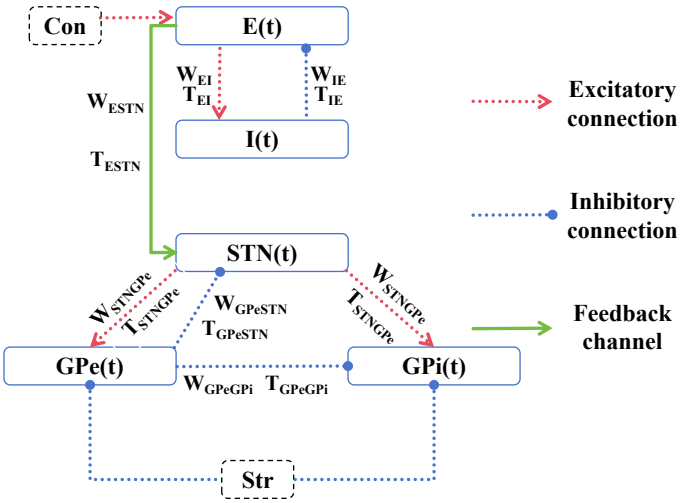

Figure 1. The schematic figure of the Cortex-BG model.

The dynamics of the Cortex-BG model are governed by the following equations [18]:

$$
\begin{aligned}
&\tau_{STN} STN'(t) = F_{STN}[W_{ESTN} E(t - T_{ESTN}) - W_{GPeSTN} GPe(t - T_{GPeSTN})] - STN(t),\\
&\tau_{GPe} GPe'(t) = F_{GPe}[W_{STNGPe} STN(t - T_{STNGPe}) - Str] - GPe(t),\\
&\tau_{GPi} GPi'(t) = F_{GPi}[W_{STNGPi} STN(t - T_{STNGPi}) - W_{GPeGPi} GPe(t - T_{GPeGPi}) - Str] - GPi(t),\\
&\tau_{E} E'(t) = F_{E}[-W_{IE} I(t - T_{IE}) + Con] - E(t),\\
&\tau_{I} I'(t) = F_{I}[W_{EI} E(t - T_{EI})] - I(t),
\end{aligned}
\tag{2.1}
$$

where $STN(t)$, $GPe(t)$, and $GPi(t)$ denote the mean firing rates of the corresponding BG nuclei, while $E(t)$ and $I(t)$ represent those of the cortical excitatory and inhibitory populations, respectively. The term τ_i (for $i = STN, GPe, GPi, E, I$) is the intrinsic membrane time constant associated with the neuron cluster i. Additionally, T_{ij} and W_{ij} represent the synaptic transmission delay and synaptic weight between neuronal clusters i and j. The constant Con corresponds to the excitatory input to E,

while Str is the external input to the striatum. Furthermore, F_i represents the activation function of the neuron cluster i, and its mathematical expression is shown below [19]:

$$F_i(in) = \frac{M_i}{1 + \left(\frac{M_i - B_i}{B_i}\right) \exp\left(\frac{-4in}{M_i}\right)}, \tag{2.2}$$

where M_i denotes the maximum firing rate achievable by neuron cluster i, while B_i represents its baseline firing rate.

2.2. Dynamic delayed feedback control

Dynamic delayed feedback control (DDFC) is applied in this study to achieve effective DBS for PD, following the methodology of Yamamoto et al. [20]. The firing rate of the STN serves as the recorded variable. A feedback signal is generated by comparing the current firing rate with its delayed counterpart. This signal is then fed into a filter, and the controller linearly combines the resulting filtered state to produce its output [16].

$$\begin{aligned} v'(t) &= \alpha(y(t) - y(t - T_{DBS})) - d_s v(t), \\ u(t) &= -K_{DBS}\, v(t), \end{aligned} \tag{2.3}$$

where $y(t)$ and $y(t - T_{DBS})$ are the firing rates at time t and $(t - T_{DBS})$, respectively. T_{DBS} represents the time delay of DBS. $u(t)$ serves as the control signal generated by the DDFC, and $v(t)$ represents the corresponding filtered state variable. The time constant d_s is defined over the interval $(0, 2)$. The feedback and linear control gains are denoted by α and K_{DBS}, respectively.

The STN is chosen as the DBS target. Furthermore, to enhance computational tractability, the model is simplified under two key assumptions. First, the time constants of all neuronal clusters are set to a common value, i.e., $\tau_i = \tau$ for all $i \in \{STN, GPe, GPi, E, I\}$. Second, the transmission delays are denoted as T_1 for delays within the cerebral cortex circuit, and T_2 for delays within the BG circuit [18, 21]. Thus, the equation for the PD model (Eq (2.1)) is given by:

$$\begin{aligned} \tau STN'(t) &= F_{STN}[W_{ESTN}E(t - T_2) - W_{GPeSTN}GPe(t - T_1) + DBS(t)] - STN(t), \\ \tau GPe'(t) &= F_{GPe}[W_{STNGPe}STN(t - T_1) - Str] - GPe(t), \\ \tau GPi'(t) &= F_{GPi}[W_{STNGPi}STN(t - T_1) - W_{GPeGPi}GPe(t - T_1) - Str] - GPi(t), \\ \tau E'(t) &= F_E[-W_{IE}I(t - T_2) + Con] - E(t), \\ \tau I'(t) &= F_I[W_{EI}E(t - T_2)] - I(t), \end{aligned} \tag{2.4}$$

where the control input $DBS(t)$ is defined as $u(t)$, and the output $y(t)$ is given by $STN(t)$ in Eq (2.4).

3. Numerical simulations

The baseline parameters for numerical simulations, listed in Table 1, are adopted from prior work [16, 22]. Specific deviations from these values are explicitly noted in the relevant sections. Based on established ranges, the membrane time constant τ was selected as 0.01 s for all neuronal clusters in

the model [19]. All computational processing was carried out in MATLAB (R2021a, The MathWorks, Natick, MA, USA).

Table 1. Summary of the parameters employed in this study.

Par	Value	Par	Value	Par	Value
τ	0.01 s	M_E	71.77 spk/s	W_{ESTN}	6.6
T_{DBS}	0.002 s	M_I	276.39 spk/s	W_{GPeSTN}	3.22
B_{STN}	17 spk/s	Con	277.94 spk/s	W_{STNGPE}	2.56
B_{GPe}	75 spk/s	Str	40.5 spk/s	W_{STNGPi}	2.56
B_{GPi}	75 spk/s	W_{EI}	3.08	W_{GPeGPi}	0.9
B_E	3.62 spk/s	W_{IE}	3.08	K_{DBS}	100
B_I	400 spk/s	M_{GPe}	7.18 spk/s	α	10
M_{GPi}	400 spk/s	M_{STN}	300 spk/s	d_s	0.5

3.1. Effect of time delays within the PD model on oscillatory dynamics

Variations in synaptic transmission delays among neurons can give rise to a spectrum of oscillatory activities in the PD model. Different frequencies of oscillations reflect abnormal activity in the BG of the brain, and by analyzing them, the severity of the disease and the response to treatment could be evaluated. Brain oscillations encompass multiple frequency bands, among which delta (I: 0.1–4 Hz), theta (II: 4–8 Hz), alpha (III: 8–13 Hz), beta (IV: 13–30 Hz), and gamma (V: >30 Hz) are the most studied [23]. Meanwhile, the STN serves as a central hub in the BG circuit and acts as the primary pacemaker for pathological oscillations [24]. Therefore, analyzing the bifurcation behavior of the firing rate of STN provides a key perspective for understanding how model parameters control the transitions between these different oscillation states. This study evaluates the influence of transmission delays on the oscillatory dynamics of the model by analyzing the firing rate of STN and oscillation frequency in response to T_1 and T_2, and further explores the role of the delayed feedback T_{DBS}.

A Hopf bifurcation occurs in the model for T_1 and T_2 when $T_{DBS} = 0.002$ s. As shown in Figure 2(a), when $T_2 = 0.002$ s, the bifurcation point for T_1 is $T_1^* = 0.011122$ s. In particular, the first oscillation to appear in the model is the beta oscillation (IV) with increasing T_1 values. When the transmission delay in the cerebral cortex circuit is sufficiently large, namely T_1, the oscillation frequency of the model gradually decreases and resting tremor (II) emerges, as shown in Figure 2(d). The value of the bifurcation point $T_2^* = 0.002274$ s for T_2 when $T_1 = 0.002$ s is obtained from Figure 2(b). Furthermore, the model transitions from a brief gamma oscillation (V) to a sustained beta oscillation (IV) with an increase in the transmission delay in the BG circuit, namely T_2 (Figure 2(e)). Additionally, fixing $T_1 = T_2 = 0.002$ s to reveal the effect of T_{DBS}, a new bifurcation diagram is observed (see Figure 2(c)), which shows the bifurcation point located at $T_{DBS}^* = 0.01111$ s. Moreover, the model transitions from a sustained gamma oscillation (V) to a beta oscillation (IV) if we enhance the delayed feedback T_{DBS} in Figure 2(f).

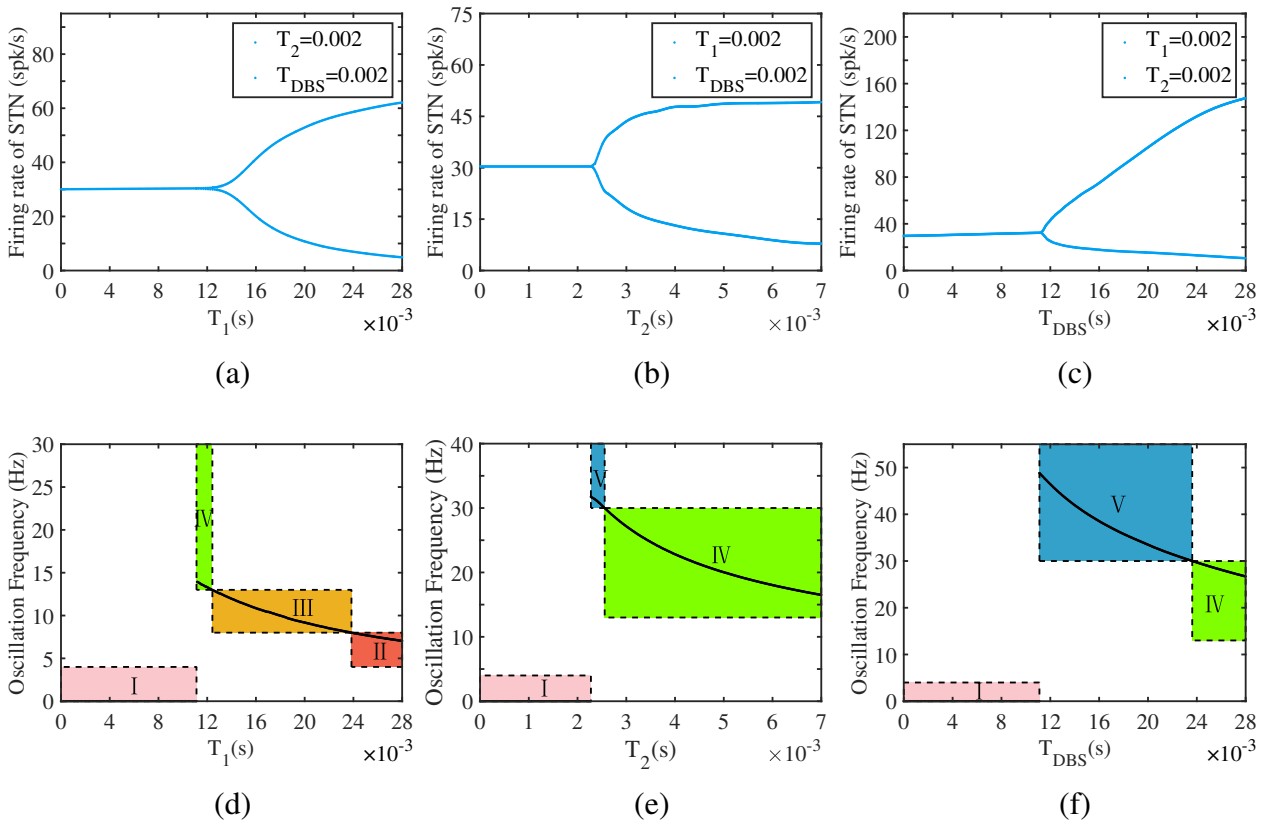

Figure 2. (a) Evolution of the firing rate of STN bifurcations with T_1 for ($T_2 = T_{DBS} = 0.002$ s). (b) Evolution of the firing rate of STN bifurcations with T_2 for ($T_1 = T_{DBS} = 0.002$ s). (c) Evolution of the firing rate of STN bifurcations with T_{DBS} for ($T_1 = T_2 = 0.002$ s). The oscillation frequency is shown in (d), (e), and (f), respectively.

The model has different states under different time delays. First, for $T_{DBS} \in [0, T^*_{DBS})$, $T_1 \in [0, T^*_1)$, and $T_2 \in [0, T^*_2)$, the PD model initially exhibits transient oscillations in the firing rate and gradually stabilizes, as shown in Figure 3(a). This behavior indicates that the model is in a stable state. Second, irrespective of T_{DBS} exceeding T^*_{DBS}, when $T_1 > T^*_1$, and $T_2 \in [0, T^*_2)$, the model exhibits oscillatory activity, with oscillations localized to the BG circuit and the cerebral cortex remaining quiescent (Figures 3(b1),(c1)). This shows that the PD model undergoes spontaneous oscillations.

In addition, when $T_1 \in [0, T^*_1)$ and $T_2 \in [0, T^*_2)$, if $T_{DBS} \in [0, T^*_{DBS})$, we observe that the BG circuit exhibits a periodic oscillation similar to that of the cerebral cortex circuit. This phenomenon is referred to as the induced oscillation state (IOS), as shown in Figure 3(b2). However, for $T_{DBS} > T^*_{DBS}$, the firing activity of the BG circuit changes, and bounded yet aperiodic oscillations with irregular fluctuations and reduced temporal regularity emerge, which indicates that excessive delayed feedback drives the BG circuit away from periodic oscillatory behavior (Figure 3(c2)). This leads to abnormalities in the synchronism and signal transmission.

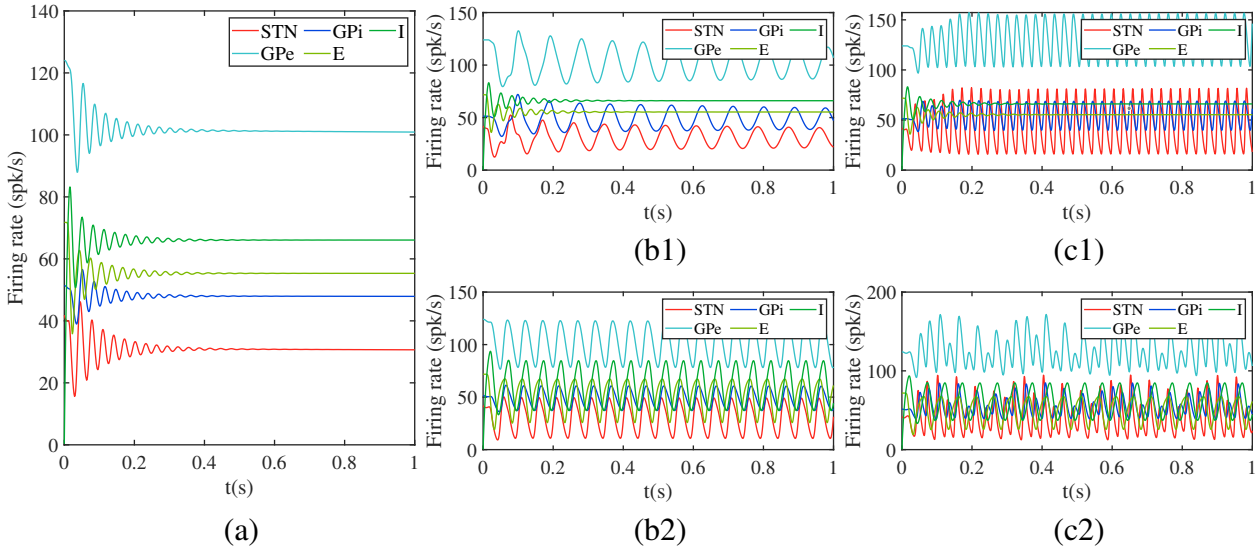

Figure 3. (a) The system is in a stable state: $T_1 = 0.002\,\text{s} \in [0, T_1^*)$, $T_2 = 0.002\,\text{s} \in [0, T_2^*)$, and $T_{DBS} = 0.002\,\text{s} \in [0, T_{DBS}^*)$. (b1) The BG circuit oscillates: $T_1 = 0.015\,\text{s} > T_1^*$, $T_2 = 0.002\,\text{s} \in [0, T_2^*)$, and $T_{DBS} = 0.002\,\text{s} \in [0, T_{DBS}^*)$. (b2) The system oscillates: $T_2 = 0.005\,\text{s} > T_2^*$, $T_1 = 0.002\,\text{s} \in [0, T_1^*)$, and $T_{DBS} = 0.002\,\text{s} \in [0, T_{DBS}^*)$. (c1) The BG circuit oscillates: $T_1 = 0.015\,\text{s} > T_1^*$, $T_2 = 0.002\,\text{s} \in [0, T_2^*)$, and $T_{DBS} = 0.018\,\text{s} > T_{DBS}^*$. (c2) The system exhibits bounded aperiodic dynamics: $T_2 = 0.005\,\text{s} > T_2^*$, $T_1 = 0.002\,\text{s} \in [0, T_1^*)$, and $T_{DBS} = 0.018\,\text{s} > T_{DBS}^*$.

3.2. Effect of synaptic weights between neural clusters on oscillation

In this section, we mainly evaluate the effect of synaptic weights on neural circuit oscillations under the DDFC ($T_{DBS} = 0.002\,\text{s}$). We set $(T_1, T_2) = (0.015\,\text{s}, 0.002\,\text{s})$, aiming to explore the influence of the synaptic weight between the E and the STN, namely W_{ESTN}. From Figure 4(a), we see that the firing rate of STN undergoes a bidirectional Hopf bifurcation when W_{ESTN} increases.

This indicates that the BG circuit undergoes a bifurcation from a stable state (SS) to an oscillatory state (OS) as a function of increasing W_{ESTN}. Furthermore, these oscillations always manifest in the alpha frequency (III) band (see Figure 4(b)). However, when W_{ESTN} exceeds a critical threshold, the oscillations collapse. This occurs because the firing rate of STN becomes excessively high, driving the BG circuit into a high-saturation stable state (HSS). These characteristics are illustrated by the time series plots in Figure 4(c). Additionally, W_{STNGPe} denotes the excitatory synaptic weight from the STN to the GPe in the BG circuit. As shown in Figure 4(d), the firing rate of STN undergoes a Hopf bifurcation with increasing W_{STNGPe}, causing the BG circuit to transition into an OS, starting from an SS as a result of the increase in W_{STNGPe}. Specifically, the STN-GPe excitatory effect strengthens, promoting oscillations within the BG circuit. These oscillations remain in the alpha frequency (III) range throughout the process as depicted in Figure 4(e). Figure 4(f) shows time series for $W_{STNGPe} = 2$ and 5, illustrating these distinct states.

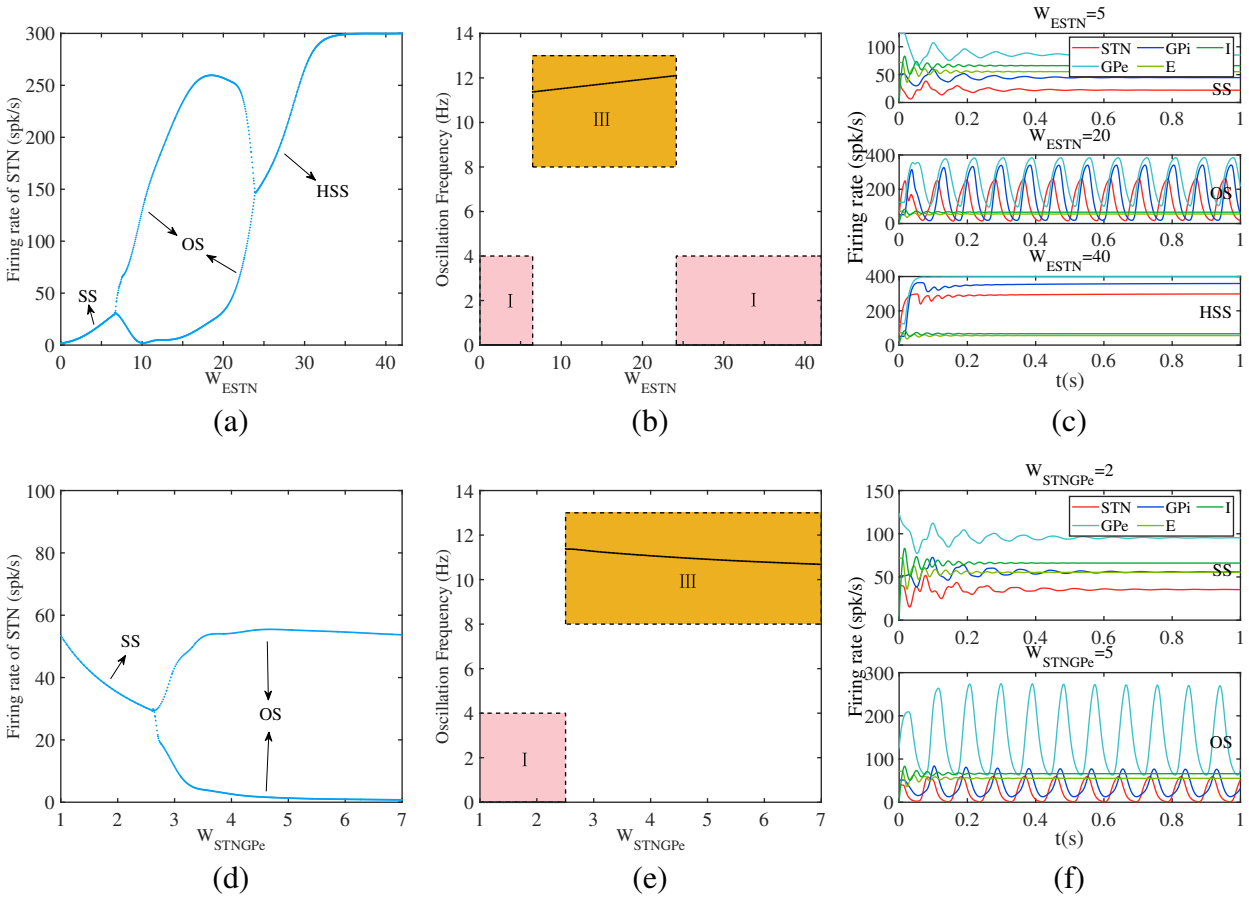

Figure 4. (a) Evolution of the firing rate of STN bifurcations with W_{ESTN}. (b) The relationship between W_{ESTN} and the oscillation frequency. (c) Set $W_{ESTN} = 5$, $W_{ESTN} = 20$, $W_{ESTN} = 40$. (d) Evolution of the firing rate of STN bifurcations with W_{STNGPe}. (e) The relationship between W_{STNGPe} and the oscillation frequency. (f) Set $W_{STNGPe} = 2$, $W_{STNGPe} = 5$.

4. Sensitivity analysis of oscillations in the PD model

Model (2.4) is a deterministic PD model, that is, a constant value is assigned to each time delay and synaptic weight. However, the activities of the system model deviate from those of the real brain owing to the intricacy of the biological brain network. Therefore, we consider the time delays along with the synaptic weights of the model as random variables uniformly distributed around the bifurcation points. For parameters whose bifurcation points are not provided, we adopt the baseline values recommended in [19] as their bifurcation points. Furthermore, we recast the PD model as a stochastic model. To quantitatively dissect how the uncertainty in these input parameters propagates to and governs the pathological oscillations, this study employs the Sobol's sensitivity analysis which is based on a polynomial chaos expansion. This variance-based method decomposes the variance of the model output, defined as the oscillation frequency of the STN, into contributions from individual input parameters and their interactions. The aim of this analysis is to determine the true impact of variability between delayed feedback and the PD model on pathological oscillations.

4.1. Polynomial chaos expansion and Sobol's sensitivity analysis

To address the inherent uncertainties, the PD model is reformulated within a stochastic framework by constructing a surrogate model based on polynomial chaos expansion (PCE) [25,26]. The surrogate model is defined as follows [21]:

$$F(X) = \sum_{\alpha \in N^d} c_\alpha \Psi_\alpha(X), \tag{4.1}$$

where $F(X)$ denotes the oscillation frequency of the STN, and $\Psi_\alpha(X)$ is a multivariate orthogonal polynomial that is based on the probability distributions associated with $X = (x_1, x_2, \ldots, x_d)$. The spectral coefficients of the PCE are represented by c_α. The truncation set is $A = \{\alpha \in \mathbb{N}^d : |\alpha| = \alpha_1 + \alpha_2 + \ldots + \alpha_d, |\alpha| \leq p\}$, where p and d are the PCE order and the dimensionality of uncertain input parameters.

This study employs Sobol's sensitivity analysis, a variance decomposition method, to evaluate the contribution of various inputs and their interactions to the model output [27]. Let $Var(F(X))$ represent the total variance of the STN oscillatory frequency output. The first-order and total-order Sobol indices, denoted S_i and S_i^T, respectively, serve as important measures for quantifying the extent to which input parameters contribute to the variability of a certain output [28]. Their formulas are shown below [21]:

$$Var(F(X)) = \sum_{i=1}^{d} Var(x_i) + \sum_{i=1}^{d} \sum_{j>i} Var(x_i, x_j) + \cdots + Var(x_1, x_2, \ldots, x_d), \tag{4.2}$$

$$S_i = \frac{Var(x_i)}{Var(F)}, \quad S_i^T = 1 - \frac{Var(F|x_i)}{Var(F)}, \tag{4.3}$$

where $Var(x_i)$ is the portion of output variance accounted for by x_i, and $Var(x_i, x_j)$ represents the variance component arising from the joint effect of x_i and x_j. $Var(F|x_i)$ is the variance of F under the condition of a fixed x_i. In calculating S_i and S_i^T, we can compute them directly using the PCE coefficients [27].

$$S_i = \frac{\sum\limits_{\alpha \in A_i} c_\alpha^2}{\sum\limits_{\alpha \in A, \alpha \neq 0} c_\alpha^2}, \quad S_i^T = \frac{\sum\limits_{\alpha \in A_i^T} c_\alpha^2}{\sum\limits_{\alpha \in A, \alpha \neq 0} c_\alpha^2}, \tag{4.4}$$

where $A_i = \{\alpha \in A : \alpha_i > 0, \alpha_{j \neq i} = 0\}$ and $A_i^T = \{\alpha \in A : \alpha_i > 0\}$.

4.2. Sensitivity analysis of transmission delays on the oscillation frequency

In this section, we use transmission delays T_1 and T_2 as uncertain parameters. To simplify the analysis, we adopt uniform distributions for the two parameters within small intervals around values of their bifurcation points (see Section 3.1). To systematically investigate the sensitivity of oscillatory frequency to parameter variations under different dynamical states, we examine two representative values of the delayed feedback parameter T_{DBS}. As shown in Table 2, Parameter Set 1 corresponds to $T_{DBS} = 0.002\,\text{s} \in [0, T_{DBS}^*)$, whereas Parameter Set 2 is defined by $T_{DBS} = 0.014\,\text{s} > T_{DBS}^*$. The PCE model for Parameter Set 1 was constructed with $d = 2$ and $p = 8$, containing 45 expansion terms. Similarly, the model for Parameter Set 2 was built with $d = 2$ and $p = 6$, containing 28 expansion terms.

Table 2. The unified boundary encompasses time delay parameters, synaptic weight parameters, and the base values of the parameters. It is important to note that $U(x_l, x_u)$ represents the uniform distribution with the lower bound x_l and the upper bound x_u.

Parameter	Baseline, x_b	Lower limit, x_l	Upper limit, x_u	$U(x_l, x_u)$
Parameter Set 1				
T_1	0.011122	0.010	0.012	$U(0.010, 0.012)$
T_2	0.002274	0.002	0.003	$U(0.002, 0.003)$
T_{DBS}	0.01111			$T_{DBS} = 0.002 \in [0, x_b)$
Parameter Set 2				
T_1	0.011122	0.010	0.012	$U(0.010, 0.012)$
T_2	0.002274	0.002	0.003	$U(0.002, 0.003)$
T_{DBS}	0.01111			$T_{DBS} = 0.014 > x_b$
Parameter Set 3				
W_{ESTN}	6.6	3.3	9.9	$U(3.3, 9.9)$
W_{STNGPe}	2.56	1.28	3.84	$U(1.28, 3.84)$
W_{STNGPi}	2.56	1.28	3.84	$U(1.28, 3.84)$
W_{GPeSTN}	3.22	1.61	4.83	$U(1.61, 4.83)$
Parameter Set 4				
T_{DBS}	0.01111	0.010	0.012	$U(0.010, 0.012)$
K_{DBS}	100	90	110	$U(90, 110)$
α	10	9	11	$U(9, 11)$

Based on the leave-one-out errors shown in Figures 5(a),(d), sample sizes of $L = 400$ and $M = 200$ were selected for Parameter Sets 1 and 2, respectively, to ensure sufficient accuracy of the PCE technique. From Figure 5(b), the first-order and total Sobol indices for both T_1 and T_2 are depicted for Parameter Set 1 ($T_{DBS} = 0.002\,\text{s} \in [0, T^*_{DBS})$), indicating that the transmission delay in the BG circuit (T_2) is more sensitive than that in the cerebral cortex circuit. Moreover, for Parameter Set 2 ($T_{DBS} = 0.014\,\text{s} > T^*_{DBS}$), the transmission delay in the cerebral cortex circuit exhibits the highest values for both the first-order (S_i) and total Sobol indices (S_i^T) (see Figure 5(e)), showing that the variance in the oscillation frequency of the STN is primarily attributable to the uncertainty in this specific parameter T_1. In addition, the reliability of the PCE models for Parameter Sets 1 and 2 is further validated in Figures 5(c),(f), respectively, through a comparison between the oscillation frequency of the STN in the PD model and the corresponding predictions from the surrogate model (PCE model). The 95% confidence intervals (estimated via 150 bootstrap replications) around the predictions underscore the precision of the surrogate model. This shift in sensitivity reflects a delay-dependent reorganization of the dominant feedback pathways in the model, whereby the delayed feedback parameter (T_{DBS}) alters the relative contribution of transmission delays in the cerebral cortex circuit and BG circuit to oscillatory frequency modulation.

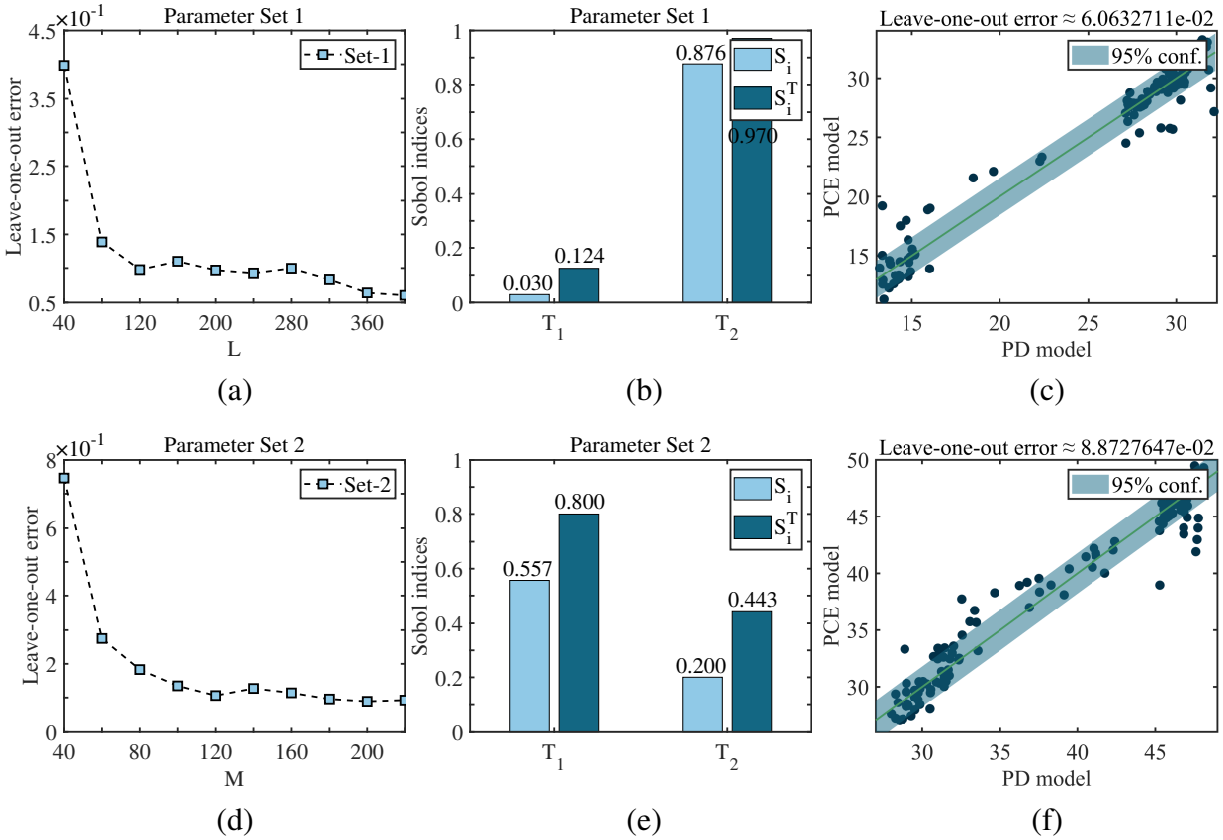

Figure 5. (a,d) Convergence of leave-one-out error estimates for the surrogate models with Parameter Sets 1 and 2, respectively. (b,e) First-order and total-order Sobol indices for Parameter Sets 1 and 2, respectively. (c,f) Comparison of the oscillatory frequency of the STN between the PD model and the PCE model for Parameter Sets 1 and 2. The solid green line indicates the 1:1 reference line, and the 95% confidence intervals were estimated from 150 bootstrap replications.

4.3. Sensitivity analysis of synaptic weights and DDFC control parameters on the oscillation frequency

In this section, we use the synaptic weights of the STN in DBS, namely W_{ESTN}, W_{STNGPe}, W_{STNGPi}, and W_{GPeSTN}, as uncertain parameters. These synaptic weights follow a uniform distribution of ±50% around the healthy values (see Table 1), with specific parameters provided in Parameter Set 3 of Table 2. The analysis is conducted under the conditions of $T_1 = T_2 = 0.002$ s and $T_{DBS} = 0.014$ s. The PCE model was constructed with $d = 4$ and $p = 3$, comprising 28 expansion terms. In addition, to further quantify the influence of DDFC control parameters on oscillation characteristics, Parameter Set 4 considers T_{DBS}, K_{DBS}, and α as uncertain parameters, modeled as independent uniform distributions (see Table 2), while synaptic weights are fixed at their baseline values, with $T_1 = 0.015$ s and $T_2 = 0.003$ s. The PCE model was constructed with $d = 3$ and $p = 5$, comprising 56 expansion terms. The time constant d_s is fixed because it mainly affects transient filter dynamics and has a weaker impact on steady-state oscillation characteristics.

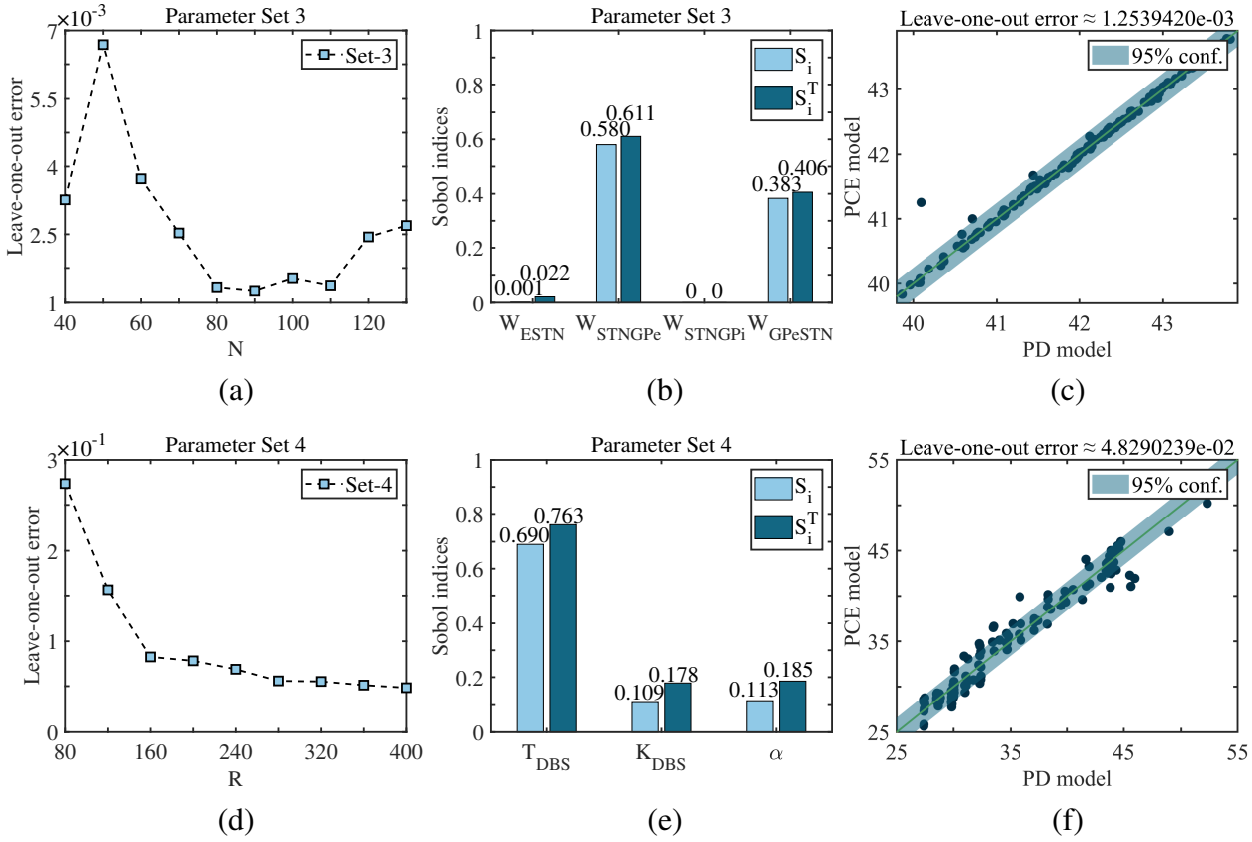

Figure 6. (a,d) Convergence of leave-one-out error estimates for the surrogate models with Parameter Sets 3 and 4, respectively. (b,e) First-order and total-order Sobol indices for Parameter Sets 3 and 4, respectively. (c,f) Comparison of the oscillatory frequency of the STN between the PD model and the PCE model for Parameter Sets 3 and 4. The solid green line indicates the 1:1 reference line, and the 95% confidence intervals were estimated from 150 bootstrap replications.

The convergence behavior of leave-one-out errors with increasing sample size is presented in Figures 6(a),(d), from which sample sizes of $N = 90$ and $R = 400$ are determined to achieve sufficient accuracy for Parameter Sets 3 and 4, respectively. W_{STNGPe} exhibits the highest values for both the first-order (S_i) and total Sobol indices (S_i^T) for Parameter Set 3 (see Figure 6(b)), indicating that the excitatory STN-GPe synaptic weight serves as the primary determinant of pathological oscillation generation under the DDFC ($T_{DBS} = 0.014$ s). Furthermore, W_{GPeSTN} within the BG circuit also exhibits high sensitivity indices, ranking second in importance. The validity of these findings is confirmed in Figure 6(c) through a comparison between the oscillation frequency of the STN in the PD model and the predictions from the PCE model, with the 95% confidence interval from 150 bootstrap replications. This highlights the pivotal role of the STN–GPe loop in shaping pathological oscillations under DDFC, showing that stimulation-induced modulation of this pathway may be particularly effective in suppressing abnormal rhythmic activity. In addition, from Figure 6(e), the first-order and total Sobol indices for T_{DBS}, K_{DBS}, and α are presented for Parameter Set 4, indicating that the delayed feedback parameter (T_{DBS}) is more sensitive than the feedback gain parameter (K_{DBS}) and the linear

control gain parameter (α), as it exhibits the largest first-order and total-effect Sobol indices. The reliability of the PCE models for Parameter Set 4 is further validated in Figure 6(f) by comparing the oscillation frequency of the STN in the PD model with the corresponding PCE predictions. The 95% confidence intervals (estimated via 150 bootstrap replications) around the predictions underscore the precision of the PCE model. This behavior can be attributed to the critical role of the feedback delay in determining the phase relationship between the control signal and intrinsic oscillatory dynamics of the STN, thereby exerting a stronger influence on oscillation regulation than gain-related parameters.

5. Discussion and conclusions

This research elucidates the mechanism linking feedback control to oscillations in PD, emphasizing the pivotal role of transmission delays and synaptic weights in generating abnormal discharges and oscillations. Results show that the delayed feedback parameter (T_{DBS}) can trigger the transition of pathological oscillations in PD, driving the system state through a dynamic progression from gamma oscillations to pathological beta oscillations and finally to complex non-periodic dynamics. Furthermore, to systematically analyze the influence of delayed feedback on pathological oscillations by modulating key transmission delays and synaptic weights, Sobol's sensitivity analysis based on PCE was employed. The analysis shows that the delayed feedback parameter (T_{DBS}) dynamically alters the contribution of the transmission delay of the cerebral cortex circuit and BG circuit to pathological oscillations. Moreover, under strong delayed feedback conditions, excitatory and inhibitory synaptic weights between the STN and GPe dominate the system dynamics, which helps to trigger oscillatory discharges of the STN. In addition, sensitivity analysis of the DDFC control parameters demonstrates that the delayed feedback parameter (T_{DBS}) plays a dominant role in modulating pathological oscillations. This finding highlights the central role of feedback delay in shaping the interaction between external control and the oscillatory dynamics of the STN, thereby providing a mechanistic explanation for the effectiveness of delay-based DBS strategies.

This study provides a scalable computational framework for analyzing the therapeutic potential of DBS by integrating dynamic delay feedback control and the Cortex-BG model. Compared with recent studies on Parkinsonian oscillations with time delays [18, 21], which mainly focus on intrinsic transmission delays and their uncertainty characteristics, the present work adopts a fundamentally different perspective by incorporating a dynamic delayed feedback control loop as a therapeutic intervention and analyzing how control parameters interact with intrinsic delays and synaptic weights to reshape oscillatory dynamics under DBS. The analysis reveals that the sensitivity of the system is not static but dynamically reconfigures with variations in delayed feedback parameters. This finding has critical implications for the design of next-generation DBS strategies. Furthermore, the sensitivity of transmission delays and synaptic weights was analyzed for the first time under conditions of dynamic delayed feedback. Despite the novelties of this paper, it is important to acknowledge some limitations of our PD model. One primary limitation is the use of a uniform parameter distribution for global exploration, which is undoubtedly a beneficial preliminary simplification. A further limitation lies in the absence of a comprehensive sensitivity analysis and optimization design for the DBS (DDFC) input parameters, which will be addressed in greater depth in subsequent studies. The further refinement of the model will require the incorporation of clinically relevant parameter distributions alongside experimental validation.

Use of AI tools declaration

The authors declare they have not used Artificial Intelligence (AI) tools in the creation of this article.

Acknowledgments

This work was supported by the Guangxi Natural Science Foundation (grant numbers 2025GXNSFAA069751, 2020GXNSFAA297240), the Natural Science Foundation of Guangxi Minzu University (grant number 2022KJQD01), and the National Natural Science Foundation of China (grant number 12062004).

Conflict of interest

The authors declare there are no conflicts of interest.

References

1. S. Safiri, M. Noori, S. A. Nejadghaderi, S. E. Mousavi, M. J. M. Sullman, M. Araj-Khodaei, et al., The burden of Parkinson's disease in the Middle East and North Africa region, 1990–2019: results from the global burden of disease study 2019, *BMC Public Health*, **23** (2023), 107. https://doi.org/10.1186/s12889-023-15018-x
2. G. E. Alexander, Biology of Parkinson's disease: pathogenesis and pathophysiology of a multisystem neurodegenerative disorder, *Dialogues Clin. Neurosci.*, **6** (2004), 259–280. https://doi.org/10.31887/DCNS.2004.6.3/galexander
3. K. A. Jellinger, The pathomechanisms underlying Parkinson's disease, *Expert Rev. Neurother.*, **14** (2014), 199–215. https://doi.org/10.1586/14737175.2014.877842
4. M. Baba, S. Nakajo, P. H. Tu, T. Tomita, K. Nakaya, V. M. Lee, et al., Aggregation of alpha-synuclein in Lewy bodies of sporadic Parkinson's disease and dementia with Lewy bodies, *Am. J. Pathol.*, **152** (1998), 879–884.
5. L. Peña-Zelayeta, K. M. Delgado-Minjares, M. M. Villegas-Rojas, K. León-Arcia, A. Santiago-Balmaseda, J. Andrade-Guerrero, et al., Redefining non-motor symptoms in Parkinson's disease, *J. Pers. Med.*, **15** (2025), 172. https://doi.org/10.3390/jpm15050172
6. S. Sveinbjornsdottir, The clinical symptoms of Parkinson's disease, *J. Neurochem.*, **139** (2016), 318–324. https://doi.org/10.1111/jnc.13691
7. G. Papagiouvannis, P. Theodosis-Nobelos, E. A. Rekka, A review on therapeutic strategies against Parkinson's disease: current trends and future perspectives, *Mini-Rev. Med. Chem.*, **25** (2025), 96–111. https://doi.org/10.2174/0113895575303788240606054620
8. V. K. Yadav, S. Dhanasekaran, N. Choudhary, D. Nathiya, V. Thakur, R. Gupta, et al., Recent advances in nanotechnology for Parkinson's disease: diagnosis, treatment, and future perspectives, *Front. Med.*, **12** (2025), 1535682. https://doi.org/10.3389/fmed.2025.1535682

9. R. Wójcik, A. Dębska, K. Zaczkowski, B. Szmyd, M. Podstawka, E. J. Bobeff, et al., Deep brain stimulation for Parkinson's disease—a narrative review, *Biomedicines*, **13** (2025), 2430. https://doi.org/10.3390/biomedicines13102430
10. D. Mellace, F. Mameli, F. Ruggiero, F. Cogiamanian, L. Borellini, A. De Sandi, et al., Triple perspective: assessing deep brain stimulation outcomes in Parkinson's disease, *BMC Neurol.*, **25** (2025), 426. https://doi.org/10.1186/s12883-025-04455-3
11. N. Malek, Deep brain stimulation in Parkinson's disease, *Neurol. India*, **67** (2019), 968–978. https://doi.org/10.4103/0028-3886.266268
12. M. G. Rosenblum, A. S. Pikovsky, Controlling synchronization in an ensemble of globally coupled oscillators, *Phys. Rev. Lett.*, **92** (2004), 114102. https://doi.org/10.1103/PhysRevLett.92.114102
13. M. Rosenblum, A. Pikovsky, Delayed feedback control of collective synchrony: An approach to suppression of pathological brain rhythms, *Phys. Rev. E*, **70** (2004), 041904. https://doi.org/10.1103/PhysRevE.70.041904
14. O. V. Popovych, C. Hauptmann, P. A. Tass, Control of neuronal synchrony by nonlinear delayed feedback, *Biol. Cybern.*, **95** (2006), 69–85. https://doi.org/10.1007/s00422-006-0066-8
15. Y. Che, T. Yang, R. Li, H. Li, C. Han, J. Wang, X. Wei, Desynchronization in an ensemble of globally coupled chaotic bursting neuronal oscillators by dynamic delayed feedback control, *Int. J. Mod. Phys. B*, **29** (2015), 1450235. https://doi.org/10.1142/S021797921450235X
16. S. Ji, Y. Che, J. Yang, S. Li, R. Wang, Suppression of beta oscillations in a Parkinson's disease model by dynamic delayed feedback control, in *2023 42nd Chinese Control Conference (CCC)*, (2023), 6818–6822. https://doi.org/10.23919/CCC58697.2023.10241154
17. H. Yang, J. Wang, Y. Wang, C. Liu, Intermittent nonlinear differential delayed feedback for suppressing synchronous oscillations of Parkinsonian state, in *2025 44th Chinese Control Conference (CCC)*, (2025), 4421–4426. https://doi.org/10.23919/CCC64809.2025.11179051
18. Q. Zeng, Y. Zheng, D. Yi, Bifurcation analysis of a Parkinson's disease model with two time delays, *Math. Comput. Simul.*, **219** (2024), 1–11. https://doi.org/10.1016/j.matcom.2023.12.007
19. A. Pavlides, S. J. Hogan, R. Bogacz, Computational models describing possible mechanisms for generation of excessive beta oscillations in Parkinson's disease, *PLoS Comput. Biol.*, **11** (2015), e1004609. https://doi.org/10.1371/journal.pcbi.1004609
20. S. Yamamoto, T. Hino, T. Ushio, Dynamic delayed feedback controllers for chaotic discrete-time systems, *IEEE Trans. Circuits Syst. I Fundam. Theory Appl.*, **48** (2002), 785–789. https://doi.org/10.1109/81.928162
21. Y. Chen, H. Nakao, Y. Kang, Emergence of pathological beta oscillation and its uncertainty quantification in a time-delayed feedback Parkinsonian model, *Chaos, Solitons Fractals*, **185** (2024), 115113. https://doi.org/10.1016/j.chaos.2024.115113
22. Y. Bi, Q. Liu, J. Zhao, W. Yang, Dynamical analyses on beta oscillations in a STN-GPE-GPI model of Parkinson's disease, *Complexity*, **2020** (2020), 4376279. https://doi.org/10.1155/2020/4376279
23. A. Perrottelli, G. M. Giordano, F. Brando, L. Giuliani, A. Mucci, EEG-based measures in at-risk mental state and early stages of schizophrenia: a systematic review, *Front. Psychiatry*, **12** (2021), 653642. https://doi.org/10.3389/fpsyt.2021.653642

24. B. Zavala, K. Zaghloul, P. Brown, The subthalamic nucleus, oscillations, and conflict, *Mov. Disord.*, **30** (2015), 328–338. https://doi.org/10.1002/mds.26072

25. F. Han, W. Wang, X. Han, W. Shi, X. Li, Investigation of sensitivity analysis of crucial dynamic characteristics of offshore wind turbine utilizing polynomial chaos expansion, *J. Offshore Mech. Arct. Eng.*, **147** (2025), 052004. https://doi.org/10.1115/1.4067797

26. M. Hamdaoui, E. M. Daya, Global sensitivity analysis of damped sandwich plates using sparse polynomial chaos expansions, *Mech. Adv. Mater. Struct.*, **32** (2025), 2807–2821. https://doi.org/10.1080/15376494.2024.2385027

27. A. Saltelli, P. Annoni, I. Azzini, F. Campolongo, M. Ratto, S. Tarantola, Variance based sensitivity analysis of model output. Design and estimator for the total sensitivity index, *Comput. Phys. Commun.*, **181** (2010), 259–270. https://doi.org/10.1016/J.CPC.2009.09.018

28. A. Kumar, A. Singh, Entropy-based groundwater quality evaluation with multivariate analysis and Sobol sensitivity for non-carcinogenic health risks in mid-Gangetic plains, India, *Environ. Geochem. Health*, **47** (2025), 186. https://doi.org/10.1007/s10653-025-02495-9

AIMS Press